Advanced Materials '93, VI / Frontiers in
Materials Science and Engineering, edited by S. Sōmiya et al.
Trans. Mat. Res. Soc. Jpn., Volume 19B

Structure of Interfaces in Crystalline Solids

T. Höche, P.R. Kenway and M. Rühle

Max-Planck-Institut für Metallforschung, Institut für Werkstoffwissenschaft, Seestr. 92,
D-70174 Stuttgart, Germany

Interfaces in materials may be grain boundaries between like crystals or phase boundaries between unlike crystals. Experimental approaches for the determination of the atomic structures of the interfaces are reviewed with emphasis on high-resolution electron microscopy (HREM). It will be shown that information on orientation relationship between the adjacent grains, the translation state and atomic relaxations can be elaborated with high precision. In a case study, the structures of one specific grain boundary in Al_2O_3 will be discussed in detail. Such experimental studies have provided a mass of structural information in recent years.

1. INTRODUCTION

Most crystals applied in materials science are used in polycrystalline form. This is not only true for metals but also for ceramics and polymers. Only semiconductors are quite often used in single-crystal form. Boundaries between the different grains or, in general, between different phases play an important and controlling role in determining the properties of different materials. Since internal interfaces play this important role, a large amount of research has been conducted on their properties over the last five decades and a rich body of literature is available [1-4].

It is helpful to distinguish between two different groups of boundaries [5] (Fig. 1.). *Homophase boundaries* are interfaces between grains of identical crystal structure and identical composition. They include grain boundaries, twin boundaries, domain boundaries and stacking faults. *Heterophase boundaries* are interfaces between regions of different crystal structure which may also vary in their chemical composition. Examples of the first kind include boundaries between coexisting allotropic modifications, for instance between grains of the tetragonal and monoclinic phase of ZrO_2. Heterophase boundaries of the second kind are present in all technical alloys and ceramics. Another group of materials which contain the latter boundaries are composites [6,7]. In all these cases, the regions adjoining the interfaces belong to different phases in the classical thermodynamic sense, therefore, the simpler term phase boundary is also often used in the literature.

In this paper experimental studies will be reported on the structure determination of interfaces by high-resolution transmission electron microscopy. Details of experimental and theoretical techniques for structure determination are reported elsewhere [8].

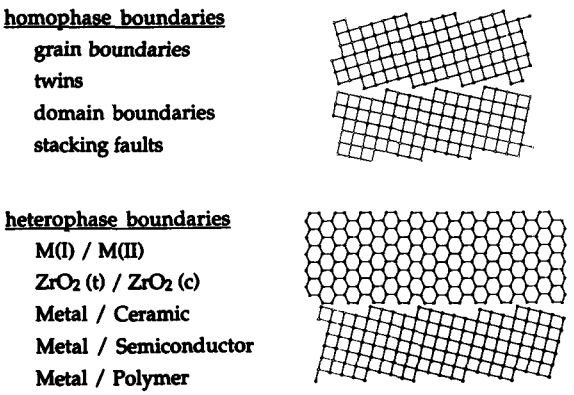

Figure 1. Classification of internal interfaces (Cahn and Kalonji, 1982)

2. EXPERIMENTAL STUDIES OF INTERFACE STRUCTURE BY HIGH-RESOLUTION ELECTRON MICROSCOPY

2.1. The Instrument

The point-to-point resolution of high-resolution electron microscopes [9] is now better than 0.17 nm for instruments with an acceleration voltage of 400 kV. The next generation of instruments pushes the resolution limit to ≈ 0.1 nm. High quality experimental images can be obtained. Nevertheless, the interpretation of the HREM micrographs is not straightforward owing to the aberration of the rotation symmetrical magnetic lenses [9,10]. Therefore, the micrographs have to be analysed by comparing them to simulated images [11,12]. Considerable advances have been made in this analysis. Methods and programs have been developed, which allow the simulation of HREM images of any given atomic arrangement. The recent developments enable us to use HREM as an important method for solving problems in materials science. Atomic structures of different lattice defects, such as phase boundaries, grain boundaries and dislocations, can be determined [8].

2.2. Comments on direct lattice imaging of distorted materials

The geometric beam path through the objective lens of a TEM is shown in Fig. 2a. Beams from the lower side of the object travel both in the direction of the incoming and diffracted beam. All beams are focused by the objective lens in the back focal plane to form the diffraction pattern. In the image plane, the image of the object is produced by interference of the transmitted and diffracted beams. Fig. 2b uses wave optics to describe physical processes which contribute to the image formation. From the lower side of the foil, a wave field emerges, called exit-face wave function, $\psi_e(x,y)$, where x and y are the object coordinates. For an undistorted lattice, $\psi_e(x,y)$ represents a simple periodic amplitude and phase distribution. The exit-face wave function of a grain boundary is a very complicated, non-periodic function due to the presence of the interface.

The wave function in the diffraction plane, $\psi_d(u,v)$, is given by the Fourier transform of $\psi_e(x,y)$: $F\{\psi_e(x,y)\}$ where u,v are the coordinates in the diffraction plane (spatial frequencies) and F{} denotes the Fourier transform. Since spherical aberration cannot be avoided with rotationally symmetrical electromagnetic lenses [9,10], the beams emerging from an object at a certain angle (Fig. 2a) undergo a phase shift relative to the direct beam. Imaging with a small defocus Δf, leads also to a phase shift, the amount of which depends on the sign and magnitude of the defocus Δf. The influence of the lens errors and the defocus on $\psi_d(u,v)$ is described by the contrast transfer function (CTF) (see [9,10]).

The wave function in the image plane, $\psi_i(x,y)$, (Fig. 2) is formed by a Fourier back-transform of the wave function in the diffraction plane multiplied by the contrast transfer function, CTF(u,v):

$$\psi_i(x,y) = F^{-1}\{\psi_d(u,v)\cdot CTF(u,v)\},$$

where F^{-1}{} denotes the Fourier back transform. $\psi_i(x,y)$ is not identical to the wave field in the object plane (exit-face wave function). If scattering to high spatial frequencies occures, the image is severely modified, since the influence of the spherical aberration increases strongly with increasing scattering angle. The modification is drastic if the beams scattered to higher angles coincide with the oscillating part of the CTF (large values of u,v). If, however, the wave vectors lie within the first wide maximum of the CTF, it can be assumed that characteristic features and properties of the object can be directly recognised in the image [8-12]. Therefore, straightforward HREM imaging requires that the first zero crossing of the

CTF under the optimum defocus (so-called Scherzer defocus, i.e., that defocus where a maximum of spatial frequencies is transmitted without noticable phase shift) is at spatial frequencies as high as possible. The point-to-point resolution is defined as the spacing that corresponds to that spatial frequency where the first zero-crossing of the CTF occures and depends mainly on the acceleration voltage and the spherical aberration of the microscope. Such imaging conditions are fulfilled for lattices with large lattice parameters (i.e., low spatial frequencies in the diffraction plane).

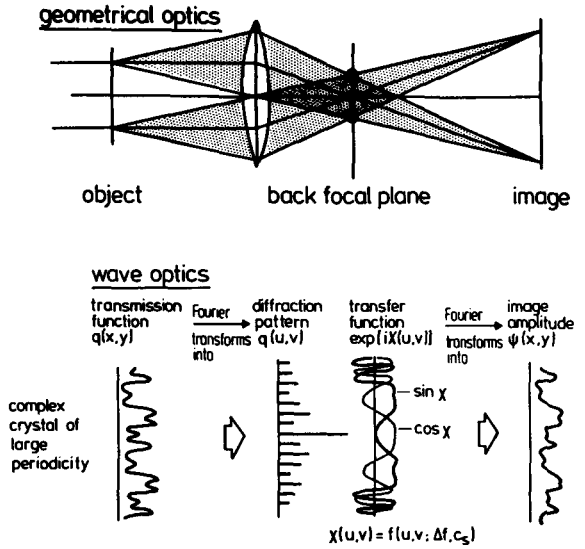

Figure 2. Image formation in an electron microscope: a) ray path and b) wave optical formulation

3. EXPERIMENTAL STUDIES OF THE STRUCTURE OF INTERNAL INTERFACES

The structure of internal interfaces can either be determined by X-ray diffraction studies such as direct diffraction studies [13] and grazing incidence X-ray scattering [14] or HREM. Most surface science techniques are not applicable for the studying of structures of interfaces in materials since for these studies the interfaces have to be intact. In contrast, surface science studies require free surface.

In this chapter we concentrate on the studies of internal interfaces by transmission electron microscopy. Transmission electron microscopy is an important tool for revealing the structure, morphology and composition of defects in crystalline materials. As shown in Fig. 3, transmission electron microscopy is split up into three independent disciplines. These include conventional transmission electron microscopy (CTEM) where the morphology, phase distribution, defect analyses and in situ experiments reveal the structure and arrangements of defects. Analytical electron microscopy (AEM) allows the determination of chemical composition with high spatial resolution. However, the limit of detectability is rather high for those techniques. Special techniques for electron spectroscopy encompass extended electron energy loss fine structure (EXELFS) studies and electron energy loss near edge structure (ELNES). With AEM composition gradients, electronic states and information on chemistry and bonding in the surroundings of specific atoms can be determined [15-17]. The usage of field emission electron sources allows the formation of spot sizes with a diameter of < 1 nm. Thus chemical information can be obtained on the near atomic level.

With high resolution electron microscopy the structure of complex materials can be analysed. A very important application of HREM is, however, the analysis of lattice defects, e.g. the atomic structure of interfaces and dislocations. One has to keep in mind that in HREM information on the projection of a crystalline specimen along a certain crystallographic axis is obtained. This requires that for the analysis of an internal interface, both grains adjacent to the interface have to be oriented such that they are parallel to a low-indexed zone axis. Small deviations (less than 1°) degenerate the

accuracy of the resultant data. In addition, the interface itself has to be parallel to the incoming electron beam (see Fig. 4).

TEM and HREM of interfaces yield several types of information (see Fig. 5). The orientation relationship between the two grains adjacent to the interface can be elaborated by selected area diffraction patterns. For heterophase boundaries it is possible to determine if a topotaxial or an epitaxial relationship exists.

From the orientation relationship one can develop the crystallography of the interfaces and can get information on the possible periodicity: either commensurate structures (periodic boundaries) or incommensurate structures (quasi-periodic boundaries) [18]. Many grain boundaries possess a commensurate structure. However, the periodicity length can be very large. Quite often, an incommensurate structure degrades to commensurate areas and defective areas [19]. Such defects are also found in heterophase boundaries, misfit dislocations and grain boundary steps.

Image simulations [11,12] are needed to interpret the HREM micrograph of Fig. 6. Matching of the perfect structures adjacent to both sides of the interface yields the determination of the translation state of both lattices. Using HREM the projected translation vector $\underline{T}$ (with the components T1, T2) can be determined with high precision.
Once the relative translation state of the two lattices has been determined, it is possible to obtain more detailed information on the interface structure and composition. This information falls broadly into three categories: (i) the terminating plane of each inorganic material (remember that these compounds can contain two or more components), (ii) the relaxations of the atoms away from their perfect lattice sites on and near to the interface, and finally (iii) the concentrations of defects and impurities on and near the interface. From these, the coordination numbers and coordination symmetries of the atoms at the interface can

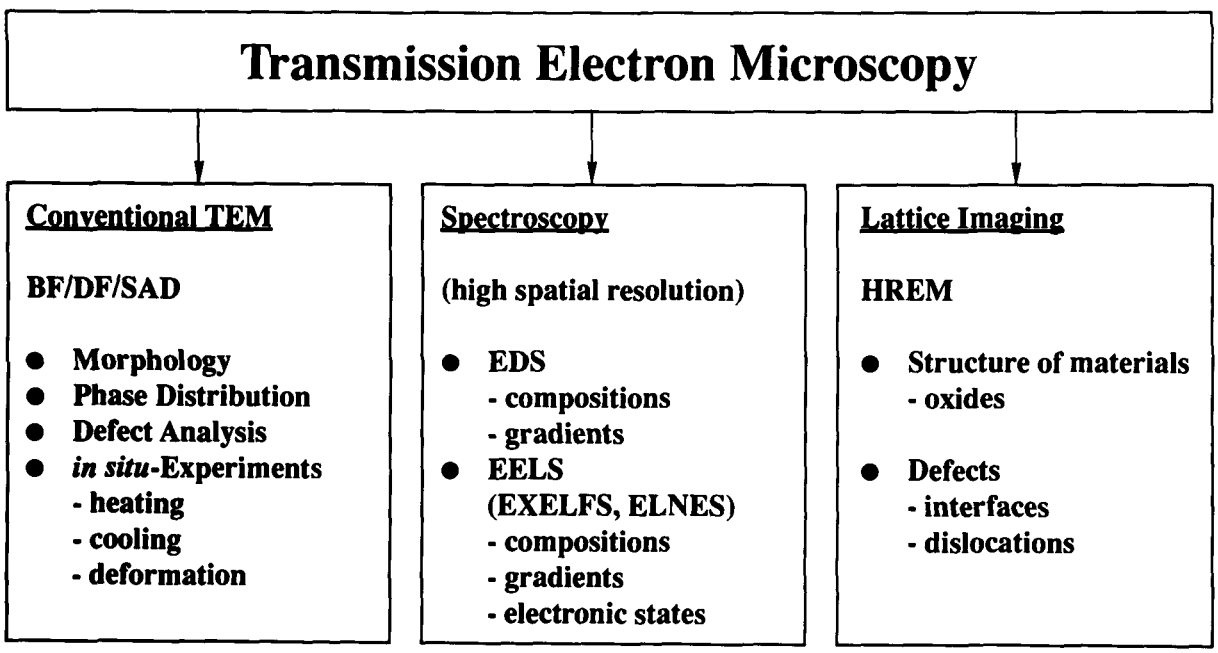

Figure 3. Classification of transmission electron microscopes (TEM)

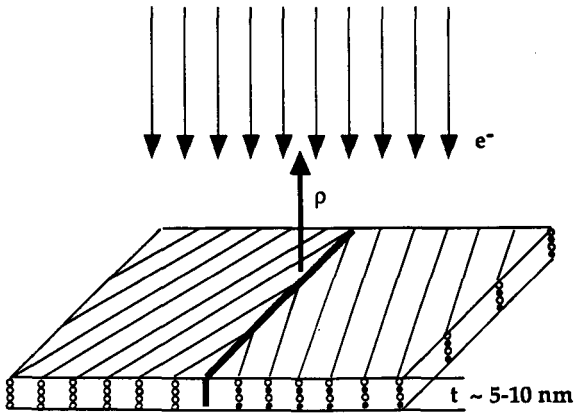

Figure 4. Specimen geometry

be ascertained, and consequently the electronic and materials properties of the interface can be studied.

The quantitative analysis of a HREM micrograph requires that experimentally obtained images are compared to simulated images. So far, this comparison has mostly been done by simple visual inspection. Recently, techniques have been developed which allow a quantitative comparison between the two images [20]. The image processing techniques require that two images are digitised. The experimental image must be noise reduced [20] and then the

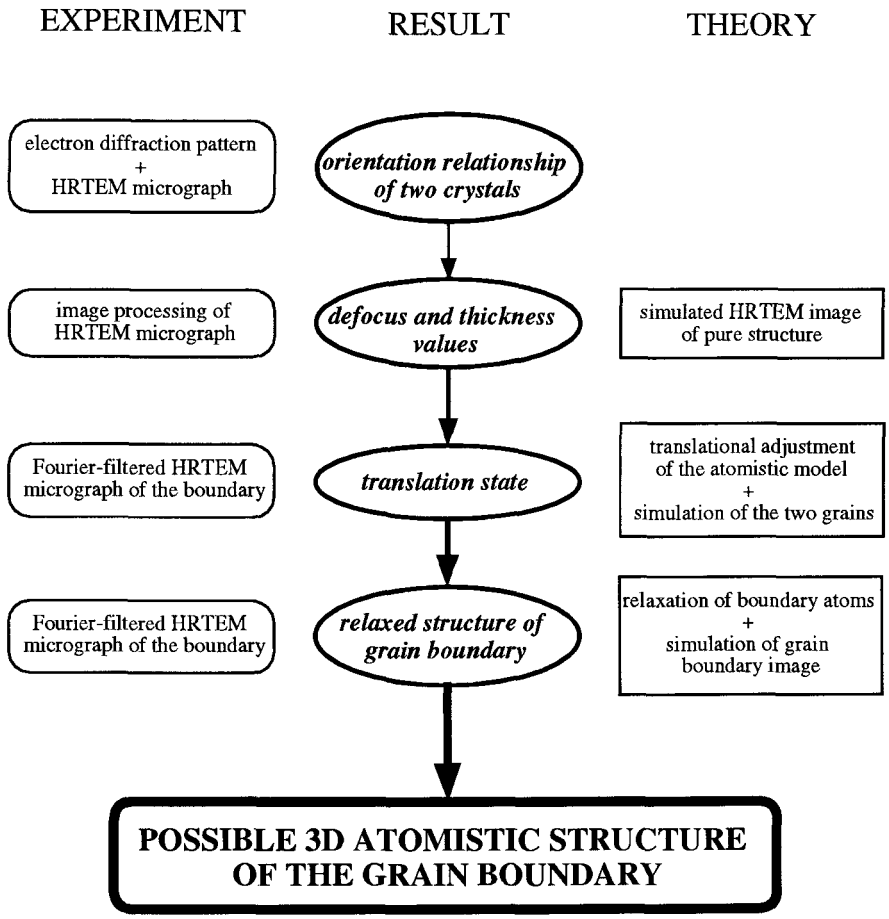

Figure 5. General scheme of who the atomistic structure of a grain boundary can be retrieved using electron microscopy

simulated image, S, and experimental image, E, are subtracted from each other to give the difference image D = E - S. Best matching is reached if the difference image does not contain any structural information, i.e. only noise is visible on D. This can be reached by shifting the positions of atomic columns in the model of the interface to those in the experiment.

This technique has been applied to several boundaries in metals and ceramics. In the following section a case study will be reported for such a study of a grain boundary in α-Al_2O_3.

4. CASE STUDY: NΣ11 BOUNDARY IN α-Al_2O_3

4.1. Introduction

The atomistic structure and distribution of internal defects such as grain boundaries are known to strongly influence the macroscopic properties of polycrystalline ceramic materials [21-25]. In order to control relevant material properties it is therefore important to characterise grain boundaries and to investigate how processing conditions can change their structures and consequently grain-boundary properties. However, commercially available polycrystalline materials with statistically distributed grain orientations and equiaxed, rounded grains are difficult to investigate using HREM owing to overlapping matrix grains and tilted grain boundaries (see Fig. 4).

In view of these difficulties and in order to study the atomistic structure of a grain boundary, a well defined interface in an ultra-pure α-Al_2O_3 bicrystal was investigated by HREM. The grain boundary discussed here is a near Σ11 grain boundary in which the two crystal halves terminate with $(0\bar{1}11)$ and $(01\bar{1}1)$ planes and which has a tilt of 35.2° about the $[2\bar{1}\bar{1}0]$-axis. Ultra-pure bicrystals were chosen because impurities will segregate to the boundary and complicate the determination of the atomistic interface structure.

These experimental investigations were correlated with theoretical studies on the grain-boundary structure [26-28]. Such a comparison enables us to unambiguously define the three-dimensional environment of the atoms in the boundary, which is a prerequisite for further calculations on defect and impurity segregation and on the electronic structure of the grain boundary.

4.2 Experimental

$Al(OH)_3$ powder was calcined using a CO_2 laser heat source until complete transformation into α-Al_2O_3 was confirmed by X-ray powder diffraction. Pellets were isopressed and fired using the laser-heating system. Growth and zone refinement (x2) of the feed rods were performed using a floating zone technique in an Ar-atmosphere. After single crystal growth, two seed-crystals were cut in defined directions and put together to form the bicrystal seed. The bicrystals were also grown in an Ar-atmosphere using the seed composed of two times zone passed feed rods. Chemical analysis showed a total impurity content of less then 59 ppm [29]. TEM foils were prepared in the usual way with an edge-on cross section of the grain boundary, i.e., the $[2\bar{1}\bar{1}0]$-direction of each crystal was parallel to the foil normal.

HREM was performed using a JEOL 4000EX microscope operating at 400 kV acceleration voltage with a point-to-point resolution of 0.17 nm (see Fig. 6). In addition, electon-diffraction and Kikuchi patterns were analysed to varify bicrystal misorientation and parallel alignment of the [2110]-zone axes.

The atomistic lattice simulations were performed using the MIDAS program [30] to calculate the grain-boundary and adhesion energy and the HREM-image simulations were calculated using the EMS-package [12]. The IMSL/IDL program was used for comparing experimentally obtained and sub-

sequently digitised images with the simulated images of theoretically suggested structure models. Noise reduction in the micrographs was achieved with a program for adaptive fourier filtering of internal interfaces [20].

5. RESULTS AND DISCUSSION

The near Σ11 (the Σ value referred to in this paper is a planar coincidence ratio Σ_p [31]) grain boundary investigated shows the expected tilt misorientation about the [2$\bar{1}\bar{1}$0]-direction as shown in the electron diffraction pattern of Fig. 6. The corresponding tilt angle was determined to be 35.2 ± 0.2 degrees.

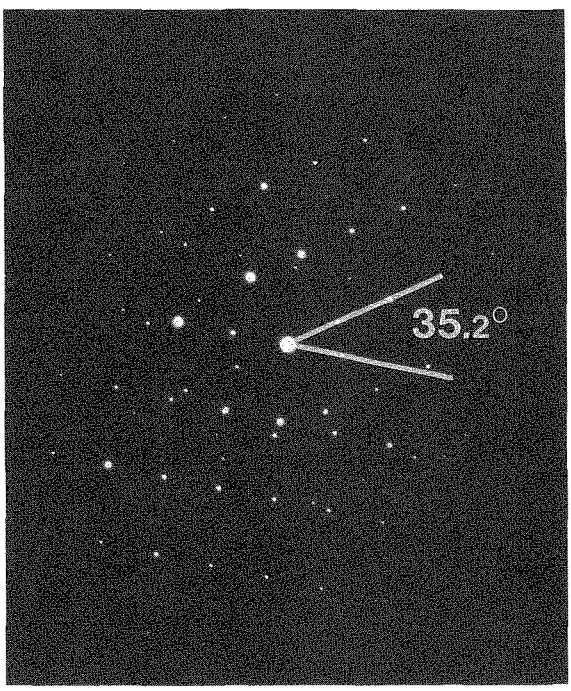

Figure 6. Electron diffraction patern recorded at the grain boundary in the α-Al_2O_3 bicrystal

It is important to note that TEM foils were prepared from two bicrystals grown with slightly different seed preorientation. Despite these minor deviations in starting orientations, the grain-boundary structure was found to be identical in both samples. The appearance of an identical grain-boundary structure in two bicrystals, grown under slightly different preorientations of the crystal seeds, seemingly suggests that the observed interface is a low energy configuration. This experimental observation is supported by theoretical arguments discussed later. The observed interface structure shows a periodicity of 1.363nm. This distance corresponds to the diagonal of the α-Al_2O_3 elementary cell projected along the [2$\bar{1}\bar{1}$0] -direction.

As already discussed in section 2, HREM images do not reveal the atomistic structure of the grain boundary directly. The atomistic structure of the interface is obtained by comparing a simulated HREM image of a model structure with the experimental HREM image.

The model of the atomistic structure of the grain boundary was generated by constructing two separate crystal slabs with surfaces terminating with (0$\bar{1}$11)- and (01$\bar{1}$1)-planes and putting them together. These two planes are not mirror related because the crystal structure of α-Al_2O_3 is not centrosymmetric. Consequently, the stacking sequences of the atomic planes perpendicular to the (0$\bar{1}$11)- and the (01$\bar{1}$1)-planes are different and are: OAlOAlO and AlOOOAl, respectively. The two slabs comprising the bicrystal can each terminate in different planes which have different compositions and atomistic environments. For example, at the (0$\bar{1}$11) surface, there are five possible terminations: three different oxygen terminations and two different aluminium terminations. The combination of the two slabs to form the bicrystal leads to 25 possible boundary configurations. As unreconstructed pure boundaries which have dipolar stacking sequences perpendicular to the interface plane are unstable, the number of these boundary combinations that needs to be considered is greatly reduced. In fact,

only one of these boundary structures is non-dipolar. This model structure was refined until the agreement between the simulated image and the observed image of the grain boundary was maximised. This was achieved by using atomistic lattice calculations. In this approach, a potential is used to calculate the energy and forces acting on the atoms. The potential used is based on the Born Model [32] of solids and includes a long-range-attractive-Coulombic interaction and a short-range-repulsive interaction. Ion polariability is also included via the Shell Model [33]. The grain-boundary-core structure was then embedded between two pure crystals terminating with $(0\bar{1}11)$- and $(01\bar{1}1)$-planes and the atoms within the grain-boundary core were relaxed until there were no net forces acting on them (mechanical equi-ibrium). The crystal blocks were also allowed to rigidly translate perpendicular and parallel to the boundary and the size of the grain boundary core was increased so that the grain boundary energy had converged. This approach is encoded in the MIDAS com-puter program [27] It was found that diffe-ent relaxed configurations of the grain boundary could be obtained by using unrelaxed configurations which differed in the relative displacements of the two crystal blocks. For comparison, the structures of three relaxed boundaries are given in Fig. 7 and their energies and excess volumes are given in Table 1. The boundary with the lowest energy of 1.7 Jm^{-2} (see boundary C in Figure 7), has the highest density of atoms in the boundary (smallest excess volume). The structure of the present boundary is such that the repulsive short range and Coulombic interactions have been minimised, and the attractive Coulombic interactions maximised. In order to analyse the complicated interface structures, image simulations of the bulkmaterial must first be matched with experimentally imaged regions of the bulk

structure	relaxed energy (Jm^{-2})	adhesion energy (Jm^{-2})
A	7.9	1.5
B	2.5	-4.0
C	1.7	-4.7

Table 1: Grain-boundary and adhesion energy of the 3 structures depicted in Fig. 7

material. This was done automatically by comparing experimental images of the bulk region with the simulated HREM images of pure alumina using image processing routines. Digitised images of both the bulk region and the interface were Fourier filtered [20] see Fig. 8. Losses due to Fourier filtering were excluded by calculating the difference picture of the filtered and unfiltered micro-graph and by analysing it with respect to changes of the image of the interface as an effect of the filtering procedure. The relative translation of the two crystals forming the grain boundary was determined by measu-ring the angles between corresponding points. To get the accuracy of relative rigid-body translation, the two crystal halves were shifted with respect to each other in the computer parallel and perpendicular to the grain boundary. The simulated HREM images of the shifted structure C indicate that the translational deviation parallel and perpendicular to the interface is reproduced to better then 0.02nm

The atomistic simulations described pre-viously provide calculated atomistic grain-boundary structures. These models have the shape of supercells containing the grain boundary and are periodic in two directions parallel to the interface. For each of the

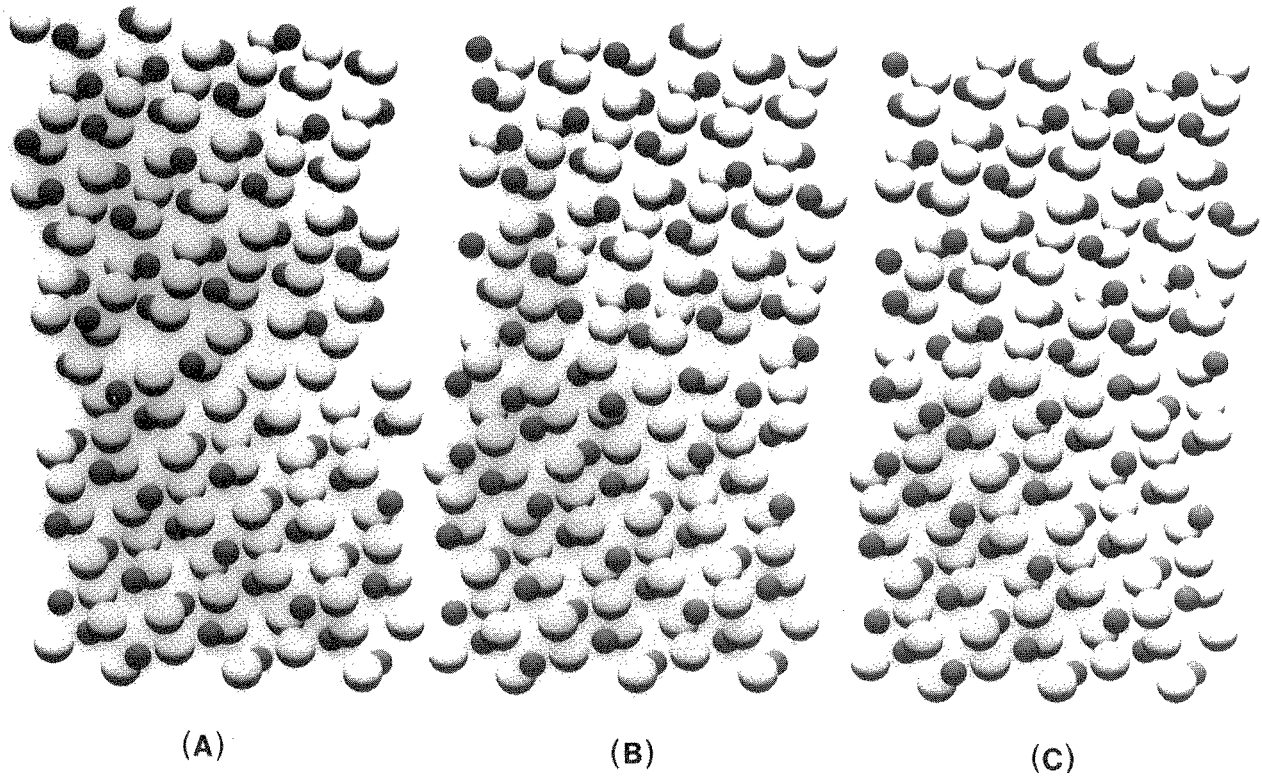

Figure 7. Three different starting structures resulting in different relaxed configurations (larger balls indicate oxygen atoms, smaller balls are aluminium atoms)

theoretically calculated model structures the resulting HREM image was simulated using optimum thickness and defocus values. The comparison of the experimental and the calculated image was done by subtracting the intensity-normalised experimental image and the shift-optimised and intensity-normalised simulated image (compare Fig. 9). The sum of the pixel intensities was used as a measure of similarity. The simulated image that showed best fit with the experimentally obtained micrograph is depicted in Fig. 8 (boundary C). As outlined by the kites, all white spots that are observed in the experimental image are reproduced in the simulated image. Some minor features of the HREM image - especially the interconnections between white spots - are not reproduced by the simulated image of structure C.

To see if these features were introduced by relaxations of the atoms in the boundary when setting up structure C, the simulated

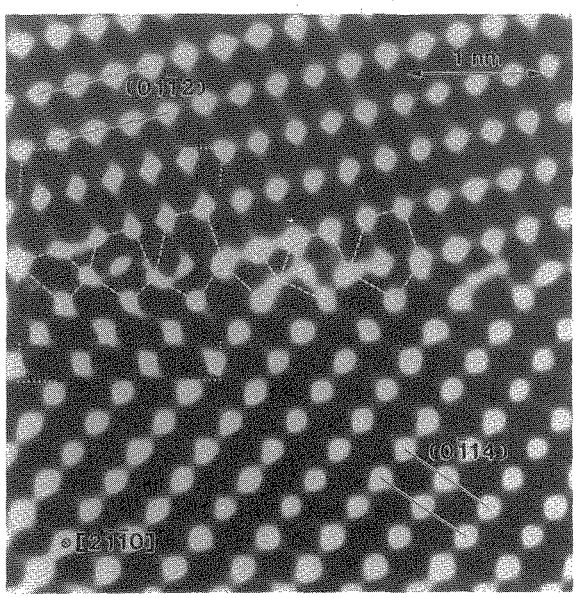

Figure 8. Fourier filtered experimental images of the near Σ 11 grain boundary in an

α-Al_2O_3 bicrystal, inset: simulated image resulting from structure C in Fig. 2 at Scherzer defocus (50nm), specimen thickness ~ 40 Å

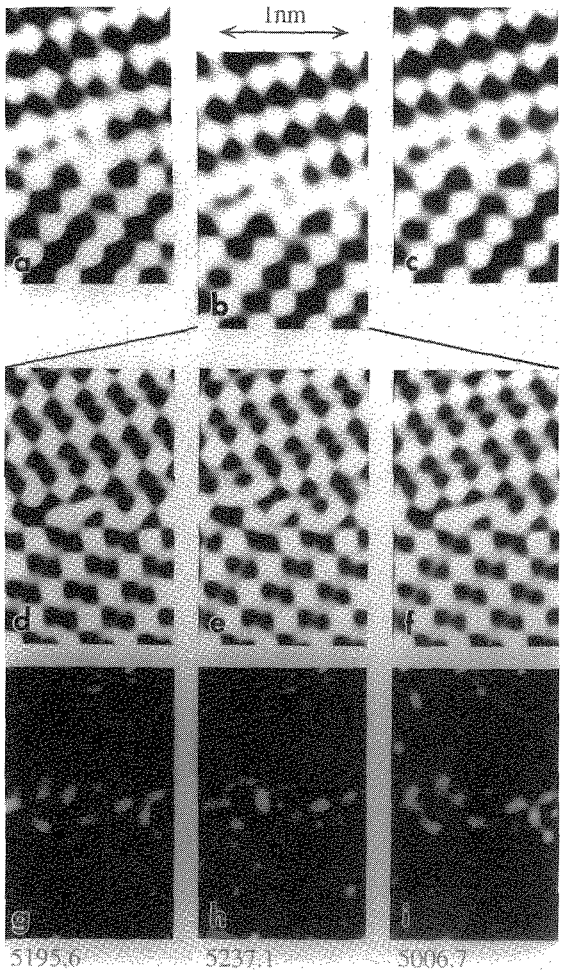

Figure 9. Comparison of experimentally observed (upper row) and simulated HREM images (middle row) by calculating the difference picture (lower row); the simulated images were compared to the experimental image b) (image a) is the unfiltered experimental micrograph, image b) the Fourier-filtered experimental micrograph and c) the experimental micrograph that was noise-reduced by translation averaging), the numbers in the lower right corner of the difference pictures indicate the sum of the pixel intensities contained in the picture, i.e. a lower number indicates a better agreement than a high number (complete dissimilarity corresponds to a value of 42,460 and identical images give a value of 0), d) corresponds to the unrelaxed structure C in Fig. 7, e) results from structure C (relaxed) and f) is the unrelaxed structure C tilted in the way described in the text

image of the unrelaxed structure of C was generated. The simulated images are compared in Fig. 9 (g and h) and it can be seen that the relaxation is not the source of the minor differences between theory and experiment.

Kikuchi patterns recorded on both sides of the boundary revealed a slight misorientation of the two crystals of 0.7 degree. To analyse whether the effect of such a misalignment of the zone axes on the image contrast is important, a supercell containing the α-Al_2O_3 interface was multiplied by 8 in the z-direction. This very large cell was cut along the interface and afterwards symmetrically tilted about 0.7 degree (0.35 degree each side) in 80 degree trace inclination to the grain-boundary normal. The contents of the wedge arising from this procedure was not altered, i.e. it consists of vacuum. New slices perpendicular to the former z-axis were cut and fed into the multislice program yielding the exit-face wave function of the tilted structure. The resulting images of the untilted and the tilted model are depicted in Fig. 9d) and 9f). The only minor effect of tilting on the image contrast is mainly due to the thinness of the investigated specimen of ~ 5nm. The importance of this part of the study is, that the degree of similarity measured in the above mentioned manner slightly increased (3%) with respect to the unrelaxed, untilted model. Presumably, the minor differences between simulated and experimental image in Fig. 8 are due to the small tilt misalignment. At present, it is not possible to incorporate the tilt into the atomistic lattice simulation of model C because the necessary supercell is too large for the available computer resources.

6. SUMMARY

High resolution electron microscopy is a powerful tool for analysing the structure of internal interfaces with high precision. As a case study, the application of HREM to α-Al_2O_3 bicrystals in conjunction with atomistic calculations of the corresponding grain-boundary structure is described. A near $\Sigma 11$ 35.2^0 tilt grain boundary with the $(0\bar{1}11)$ // $(01\bar{1}1)$ interface was studied. Good agreement between experimentally observed and theoretically calculated HREM images was obtained for the most stable structure (grain boundary energy of 1.7 Jm^{-2}) that was considered. Rigid-body translations parallel and perpendicular to the interface were reproduced to better than 0.02nm.

ACKNOWLEDGEMENTS

This work was supported by Stiftung Volkswagenwerk under contract number I/67518. P.R.K. acknowledges the financial support of an Alexander-von-Humboldt fellowship. H.-J. Kleebe, now at University of Bayreuth, is gratefully acknowledged for very fruitful discussions. The authors thank P.A. Morris, currently working at Du Pont, Wilmington, Delaware, U.S.A., who prepared the ultra-pure bicrystals.

REFERENCES

1. M. Rühle, R.W. Balluffi, H. Fischmeister, S.L. Sass, (eds.), Int. Conf. on the Structure and Properties of Internal Interfaces, J. de Physique 46, Coll. C4, 1984.
2. R. Raj, S.L. Sass (eds.), Interface Science and Engineering '87, Int. Conf. Lake Placid, Colloque C5. Les Ulis; Les Editions de Physique 49, 1987.
3. M. Aucouturier (ed.), Proc. Int. Congr. Intergranular and Interphase Boundaries in Materials. J. de Phys. 51, Colloq. C1. Les Ulis: Les Editions de Physique, 1989.
4. Ph. Komninou and A. Rocher (eds.), Proc. Int. Congr., Intergranular and Interphase Boundaries in Materials iib'92, Mat. Sci. Forum, 126, 1993.
5. J.W. Cahn, G. Kalonji. in: Solid-Solid Phase Transformations: D. Warren, H.I. Aaronson, D.E. Laughlin, R.F. Sekerka, C.M. Wayman (eds.). Warrendale: The Metallurgical Society of AIME, (1982) 3.
6. Y. Ishida (ed.), Fundamentals of Diffusion-Bonding, Elsevier, Amsterdam, 1987.
7. S. Suresh, A. Needleman (eds.), Proc. Symp. Intefacial Phenomena in Composites, Newport. Mat. Sci. Eng. A 107, (1988) 280.
8. M.W. Finnis and M. Rühle, in: Materials Science and Technology, Vol. 1, V. Gerold (ed.), VCH Weinheim, 1993.
9. P.B. Hirsch, A. Howie, R.B. Nicholson, D.W. Pashky, M.J. Whelan, Electron Microscopy of the Crystals: R.E. Krieger (ed.). New York: Huntington, 1977.
10. J.C.H. Spence, Experimental High-Resolution Electron Microscopy, 2nd ed., Oxford: Oxford University Press, 1988.
11. M.A. O'Keefe, "Electron Image Simulation: A Complimentary Processing Technique", Electron Optical Systems. Chicago: SEM, Inc., (1985) 209.
12. P.A. Stadelmann, Ultramicroscopy 21, (1987) 131.
13. I. Majid, P.D. Bristowe, R.W. Balluffi, Phys. Rev. B40 (1989) 2779.
14. K.S. Liang, Acta Metall. Mater. 40 (1992) 143.
15. R.F. Egerton, Electron-Energy-Loss Spectroscopy in the Electron Microscope, Plenum Press, New York and London, 1986.
16. J.D.C. Joy, A.D. Romig, Jr. and J.I. Goldstein (eds.). Principles of Analytical Electron Microscopy, Plenum Press, New York and London, 1986.
17. M.M. Disko, C.C. Ahn and B. Fult (eds.), Transmission Electron Energy Loss Spectrometry in Materials. The Minerals, Metals & Materials Society, 1992.

18. P. Busek, J. Cowley, L. Eyring (eds.) High Resolution Transmission Electron Microscopy, Oxford University Press, Oxford, 1988.
19. A.P. Sutton. in: Phase Transitions, Vol. 16 & 17: A.;. Glazer (ed.), Gordon and Breach, 1989.
20. G. Möbus, G. Necker and M. Rühle, Ultramicroscopy, 49 (1993) 46.
21. M.P. Harmer, Adv. Ceram. 12 (1983) 779.
22. J. Bennison and M.P. Harmer, J. Am. Ceram. Soc. 66 [5] (1983) C-90.
23. R.D. Bagley and D.L. Johnson, Adv. Ceram. 12 (1983) 666.
24. J. Rödel and A.M. Glaeser, J. Am. Ceram. Soc. 73 [11] (1990) 3292.
25. W.R. Cannon, Adv. Ceram. 12 (1983) 741.
26. T. Höche, P.R.Kenway, M. Rühle, MRS Proceedings, Vol. 295, (1993).
27. T. Höche, P.R.Kenway, H.-J. Kleebe, M. Rühle, to be published in J. Am. Ceram. Soc. 76 (1994).
28. P.R. Kenway, to be published in J. Am. Ceram. Soc. 76 (1994).
29. P.A. Morris, Ph.D. Thesis, M.I.T. Cambridge, MA, 1986.
30. P.W. Tasker, Harwell Report R9130, Harwell Lab. UK, 1978.
31. R.P. Fortunée, M.S. Thesis, Case Western University, Cleveland, OH, 1981.
32. M. Born and K. Huang, Dynamical Theory of Crystal Lattices, Oxford University Press, Oxford, 1954.
33. B.G. Dick and A. W. Overhauser, Phys. Rev. 122 (1958) 90.

Manfred Rühle is director at the Max-Planck-Institut für Metallforschung in Stuttgart, Germany, and professor at the University of Stuttgart.

He received his diploma (M.S.) and his Ph.D. in physics from the University of Stuttgart. Prior to joining the Max-Planck-Institut für Metallforschung in Stuttgart in 1989, he was a research associate at the same institute until 1986. In 1986 he joined the Materials Department of the University of California in Santa Barbara until 1989. His major publications include microstructural characterization of advanced ceramics, such as phase transformations in zirconia, grain boundary structures in ceramics as well as structure and properties of heterophase boundaries. He is best known for his extensive work on *in-situ* observations on stress-induced martensitic transformations in zirconia. Recently, he reported experimental studies on the atomistic structure of metal/ceramic interfaces. He authored and coauthored more than 200 papers.